Title	Reactivity of sub 1 nm supported clusters: (TiO2)(n) clusters supported on rutile TiO2 (110)
Authors	Iwaszuk, Anna;Nolan, Michael
Publication date	2011-02-18
Original Citation	Iwaszuk, A. and Nolan, M. (2011) 'Reactivity of sub 1 nm supported clusters: (TiO2)n clusters supported on rutile TiO2 (110)', Physical Chemistry Chemical Physics, 13(11), pp. 4963-4973. doi: 10.1039/C0CP02030C
Type of publication	Article (peer-reviewed)
Link to publisher's version	10.1039/C0CP02030C
Rights	© The Royal Society of Chemistry 2011. This is the Accepted Manuscript version of a published work that appeared in final form in Physical Chemistry Chemical Physics. To access the final published version of record, see http://pubs.rsc.org/en/content/articlepdf/2011/cp/c0cp02030c
Download date	2024-04-17 20:59:30
Item downloaded from	https://hdl.handle.net/10468/1668

Reactivity of sub 1nm supported clusters: $(TiO_2)_n$ clusters supported on rutile TiO_2 (110)

Anna Iwaszuk and Michael Nolan[*]

Metal oxide clusters of-sub nm dimensions dispersed on a metal oxide support are an important class of catalytic materials for a number of key chemical reactions, showing enhanced reactivity over the corresponding bulk oxide. In this paper we present the results of a density functional

10 theory study of small sub-nm TiO_2 clusters, Ti_2O_4, Ti_3O_6 and Ti_4O_8 supported on the rutile (110) surface. We find that all three clusters adsorb strongly with adsorption energies ranging from -3 eV to -4.5 eV. The more stable adsorption structures show a larger number of new Ti-O bonds formed between the cluster and the surface. These new bonds increase the coordination of cluster Ti and O as well as surface oxygen, so that each has more neighbours. The electronic structure shows that

15 the top of the valence band is made up of cluster derived states, while the conduction band is made up of Ti 3d states from the surface, resulting in a reduction of the effective band gap and spatial separation of electrons and holes after photon absorption, which shows their potential utility in photocatalysis. To examine reactivity, we study the formation of oxygen vacancies in the cluster-support system. The most stable oxygen vacancy sites on the cluster and show formation energies

20 that are significantly lower than in bulk TiO_2, demonstrating the usefulness of this composite system for redox catalysis.

1. Introduction

Nanoparticles of metal oxides show very different behaviour to the bulk oxide. In particular, at the sub-nm length scale,
25 they show no features that can be obviously derived from the bulk oxide, including band gaps and reactivity that can be tuned by cluster size[1-4]. Supported sub-nm metal oxide clusters dispersed on oxide supports are widely used in catalysis[4-14], a paradigm example being supported vanadium
30 oxide (VO_X)[14-17]. The interface between the cluster and the support is thought to be important for the resulting properties. Recently small nanoclusters of oxides have been deposited on the rutile TiO_2 (110) surface; this includes $(WO_3)_3$ [5-18], CeO_X [7,19,20], Nb_2O_5 [21,22], as well as WO_X on ZrO_2 [23] and IrO_X [12] on
35 Fe_2O_3. In addition, composite structures formed between two different oxides are being explored with an emphasis on the resulting band structures and photocatalysis; recent examples include Fe_2O_3/TiO_2 [24], FeO_x-TiO_2 [11] and doped-anatase/doped-rutile TiO_2 [25,26].
40 Recently Rodriguez *et al.* have studied well-defined Ce_2O_4/Ce_2O_3 (CeO_X) species on rutile TiO_2 (110) as a promising WGS catalyst using experiment and modelling[19,20,27]. The supported cluster is formed by depositing Ce metal onto the TiO_2 surface and oxidising. The
45 supported CeO_X species is more reducible than the bulk and leads to a strong reduction in the energy barrier for water dissociation, considered the rate limiting step in the WGS reaction.

$(WO_3)_3$ nanocluster on TiO_2 has been studied for catalytic
50 dehydrogenation of propanol[5,18] and a structure of the supported cluster has been proposed. A later first principles density functional theory study has examined a number of models of this system to assign the most likely adsorption structure[28].

55 The application of supported oxide nanoclusters in catalysis is a very active field. The composites in refs. [11,24,25,26] have focussed instead on their photocatalytic properties. The composite systems show enhanced photocatalytic activity over the individual compenents, which is encouraging for the
60 development of suitable materials based on TiO_2. A key finding is that the valence and conduction band of the composite systems are found on different parts of the composite. For example, in ref. 25, it is shown clearly that the valence band has its origin in rutile TiO_2, while the
65 conduction band has its origin from anatase TiO_2 – this then leads to separation of electrons and holes after photoexcitation, thus reducing recombination. A similar finding has been published for FeO_XTiO_2 [11,24]. Thus, nanocluster-support material systems show great promise for a
70 number of interesting technology areas.

From the theory side, there have been many studies of small oxide cluster structures supported on a metal oxide, for example[7,14,19,20,27-34], which have elucidated the nature of the bonding between the two species and the impact of formation
75 of the interface between the two species. Deskins *et al.* have studied the interface between rutile and anatase surfaces[35].

Other work has considered these structures for catalytic reactions. Metiu and co-workers have studied a number of oxidised metals adsorbed at the rutile TiO_2 (110) surface,
80 namely Mo, V, Cr, which they found to be most stable as MO_3 clusters[29,30]. These were found to be reactive centres for oxidative dehydrogenation of methanol[29] and oxidation of CO[30]. Recently a Ce_2O_4 cluster was studied on different metal oxide supports, i.e. CeO_X-Al_2O_3 and CeO_X-ZrO_2 [31], where the

emphasis was on the effect of the support on the reactivity of the system.

We are interested in studying TiO_2 clusters on TiO_2 surfaces as new photocatalyst materials and reactive catalytic centres for reactions such as WGS or methanol oxidation. In this paper, we study TiO_2 clusters, $(TiO_2)_n$, where n = 2, 3 and 4, that are supported on a rutile TiO_2 (110) surface. Experimental synthesis and deposition of supported metal oxide clusters is possible *via* cluster deposition or by metal deposition and oxidation, as outlined above, but to date has not been described for TiO_2 supported on TiO_2. Until now cluster deposition has been used mainly for assembly of porous thin films, however it is a possible approach to deposit small well defined clusters on an oxide substrate. Until such experiments are performed, first principles modelling can be used to study the properties of supported metal oxide clusters.

For reactions such as CO oxidation, a common descriptor to understand the ability of a metal oxide to catalyse this reaction is the oxygen vacancy formation energy[36-38], i.e. the energy needed to remove a neutral oxygen atom from the oxide. This is a good descriptor since the CO oxidation reaction generally undergoes a Mars van Krevelen mechanism[39], in which CO removes oxygen from the catalyst and the oxygen is returned by adsorption of O_2 from the atmosphere; the key step is the initial removal of oxygen from the catalyst by CO. In this regard, undoped TiO_2 should not be a very good catalyst since the formation energy of an oxygen vacancy in the (110) surface is 3.66 eV from DFT+U[40,41], however an energy from periodic B3-LYP studies was not given[41,42]. It is possible that small clusters of TiO_2 could be more favourable for oxygen vacancy formation, as it is generally the case that small clusters are more reactive than their bulk counterpart; this has been discussed for ceria clusters recently[43].

We determine stable adsorption configurations for the TiO_2 clusters on the rutile (110) surface and study the electronic properties of these structures as well as their reactivity in terms of oxygen vacancy formation. We find (i) the clusters bind strongly to the surface, (ii) have a reduced effective band gap and (iii) removal of oxygen from the cluster is more favourable than from the surface or the bulk. These findings have important implications for potential photocatalytic activity and for chemical reactivity.

2. Methodology

To model the rutile (110) surface, we use a three dimensional periodic slab model and a plane wave basis set to describe the valence electronic wave functions within the VASP code[43]. The cut-off for the kinetic energy is 396 eV. For the core-valence interaction we apply Blöchl's projector augmented wave (PAW) method[45], with Ti described by 4 valence electrons and oxygen by 6 valence electrons. We use the Perdew-Wang91 approximation to the exchange-correlation functional[46]. k-point sampling is performed using the Monkhorst-Pack scheme, with sampling at the Γ-point; in ref. 47 a comparison of a (2x2x1) sampling grid and Γ-point sampling for Ti adsorbed at the same rutile (110) surface

showed that both gave consistent results. Results from these tests show minimal influence of the k-point sampling grids tested.

The (110) surface is made up of neutral O-Ti-O tri-layers along the slab and no dipole moment is present upon cleaving. It has rows of two-fold coordinated bridging oxygens (denoted O^{br}) terminating the slab, and in the next layer there are two types of Ti: 6-fold coordinated Ti (Ti^{6f}) and exposed 5-fold coordinated Ti (Ti^{5f}). For this surface, a (2 x 4) surface cell expansion is employed, while the slab is 6 O-Ti-O layers thick and the vacuum gap is 12 Å; this slab model has been used in previous work[47]. All calculations are spin polarised with no restrictions on the overall spin.

The bare TiO_2 surface, the free TiO_2 clusters and the clusters adsorbed at the (110) rutile surface are calculated in the same periodic supercell, with the same plane wave cut off energy, the same k-point sampling grid, the same DFT approach and the same PAW potentials, ensuring consistency between calculations. To study cluster adsorption, the clusters are positioned in a number of configurations at the (110) surface and then a full relaxation is performed within a fixed supercell. The adsorption energy is computed from

$$E^{ads} = E((TiO_2)_n\text{-}TiO_2) - \{ E((TiO_2)_n) + E(TiO_2) \} \quad (1)$$

Where $E((TiO_2)_n\text{-}TiO_2)$ is the total energy of the cluster supported on the surface, and $E((TiO_2)_n)$ and $E(TiO_2)$ are the total energies of the free cluster (made up of n TiO_2 units) and the bare surface; a negative adsorption energy signifies that cluster adsorption is stable.

To study oxygen vacancies, we remove one oxygen atom from a number of sites on the cluster, oxygen atoms shared by the cluster and bridging oxygen atoms from the surface and allow full relaxation. The formation energy of an oxygen vacancy in the cluster is given by:

$$E^{vac} = [E(TiO_{2-x})_n\text{-}TiO_2) + E(1/2O_2)] - E((TiO_2)_n\text{-}TiO_2) \quad (2)$$

and in the support surface by:

$$E^{vac} = [E(TiO_2)_n\text{-}TiO_{2-x}) + E(1/2O_2)] - E((TiO_2)_n\text{-}TiO_2) \quad (3)$$

Throughout, a positive energy signifies that there is a cost for formation of an oxygen vacancy. To describe oxygen vacancy formation in the cluster-support system, we apply the DFT+U approach[48,49], which adds a Hubbard U correction to describe the reduced Ti states that result from vacancy formation. The need for an approach like DFT+U or hybrid DFT (which is too costly in a plane wave basis set for the present calculations with up to 300 atoms) to describe localised reduced cation states is defective systems is well known and has been the subject of a number of papers[40,41,50-53]. We have tested DFT and DFT+U with U = 3 eV[47] and U = 4.5 eV[27] on a number of oxygen vacancy structures and find that, of the two values of U, U = 4.5 eV is a more suitable approach to describe defective TiO_2, in particular the localisation of charge on Ti species after removal of oxygen, and this value of U is also consistent with values of U in the literature. Some extra details of the comparison between DFT and DFT+U are presented in the supporting information. Calculations of non-defective systems also use DFT+U with U = 4.5 eV for consistency between the two sets of calculations.
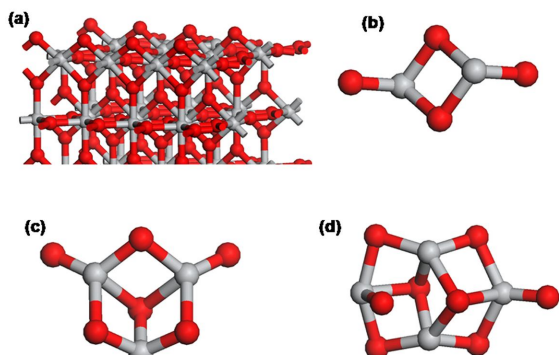
Fig.1 (a): Atomic structure of the bare TiO$_2$ (110) surface .Structure of the free (b) Ti$_2$O$_4$, (c) Ti$_3$O$_6$ and (d) Ti$_4$O$_8$ clusters. In this and subsequent figures, Ti is grey and O is red.

3. Results

3.1 Adsorption Structures of (TiO$_2$)$_n$ clusters on Rutile TiO$_2$(110)

In figure 1 we show the atomic structure of the bare TiO$_2$ (110) surface and the free Ti$_2$O$_4$, Ti$_3$O$_6$ and Ti$_4$O$_8$ clusters. The cluster structures shown in figure 1 are global energy minima obtained from Monte Carlo sampling and are similar to cluster structures in earlier studies[54,55]. In the clusters, the major different with regard to bulk TiO$_2$ is the non-bulk environment experienced by Ti and O. For example, Ti atoms show reduced coordination, with 3-coordinated Ti in Ti$_2$O$_4$ and 4 and 5 coordinated Ti present in Ti$_3$O$_6$ and Ti$_4$O$_8$; there are no 6 coordinated Ti atoms in these clusters. Oxygen can be 1, 2 or 3 coordinated and in each cluster there is always at least one terminal oxygen bound to one Ti. The majority of oxygen atoms are two coordinated.

Ti-O distances are therefore shorter than in the bulk, e.g. in the Ti$_2$O$_4$ cluster, Ti-O distances are 1.68 Å and 1.86 Å to terminal O and 2-fold coordinated O. We compared Ti$_2$O$_4$, Ti$_3$O$_6$, Ti$_4$O$_8$ structures with two codes, namely Turbomole (PBE and PW91 exchange-correlation functionals, with a TZVPP basis set on all atoms) and VASP. For all clusters after relaxation with the PBE and PW91 exchange-correlaion functional (common to both codes) we found that two methods show the same configurations with the bond lengths showing differences of around 0.02 Å.

Comparing the structure of Ti$_3$O$_6$ and Ti$_4$O$_8$ clusters we observe that both clusters have two terminal oxygen atoms b with Ti, with Ti-O distances 1.68 Å and 1.69 Å for (Ti$_3$O$_6$) and 1.68 Å and 1.78 Å for Ti$_4$O$_8$. For the three-coordinated oxygen atoms the Ti-O distances are 2.08 Å (the longest) and 1.84 Å (the shortest) and two-coordinated oxygen atoms bind to Ti with distances 2.01 Å (the longest) and 1.77 Å (the shortest).
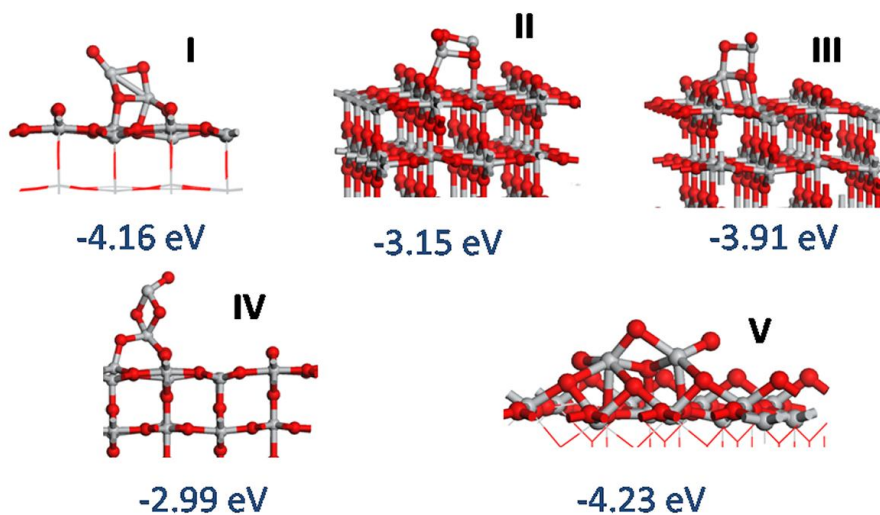

Fig2 Relaxed adsorption structures and computed adsorption energies for Ti$_2$O$_4$ deposited on the TiO$_2$ (110) surface. The roman numerals signify the numbering of the cluster structures. The adsorption energies are given under each structure in eV, computed from eq. (1). The colour scheme is the same as figure 1.
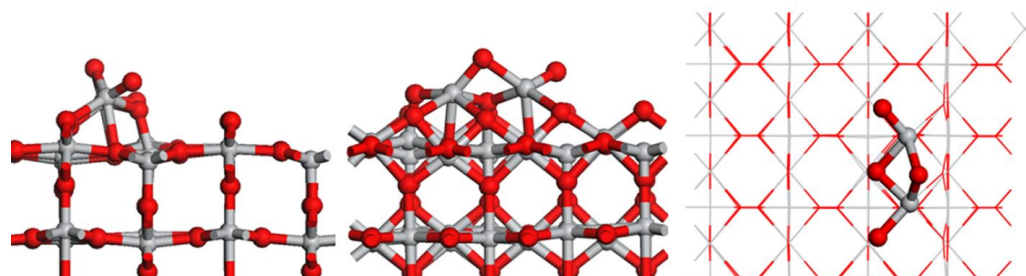
Fig. 3 Atomic structure of adsorption structure V for Ti$_2$O$_4$ adsorbed at the TiO$_2$ (110) surface showing different views. The left panel is a side view, the middle panel is a front view and the right panel is looking down on the surface. In the right panel, the atoms of the surface are represented as lines to highlight the structure of the adsorbed Ti$_2$O$_4$ cluster.

The TiO$_2$ clusters deposited on the (110) surface are chosen to be stoichiometric, since such clusters are more stable in the gas phase than reduced clusters. Thus, fully oxidised nanoclusters of TiO$_2$ are a good starting point. The surface cell expansion is large enough that the clusters are deposited in an isolated fashion.

In figure 2, we show five stable (as measured by negative adsorption energy) adsorption structures for Ti$_2$O$_4$ adsorbed on the rutile TiO$_2$ (110) surface, numbered I, II, III, IV and V. For the most stable structures of Ti$_2$O$_4$ supported on TiO$_2$, i.e. structures I and V, we have also run some ab initio molecular dynamics simulations – for 2 ps, in the NVE ensemble, at a temperature of 500 K – to allow a wider configuration space to be sampled. Upon relaxing the MD structures (heat and quench approach) we find little change to the structures shown in figure 2, indicating that these are stable adsorption structures. A similar test for the other supported clusters (Ti$_3$O$_6$ and Ti$_4$O$_8$) also shows that the structures presented for these clusters are stable and lower energy structures were not found. For each cluster, we will focus the remainder of the paper on the most stable adsorption structure.

In depositing TiO$_2$ clusters, we find that maximizing the number of new Ti-O bonds is a good guide to the relative stability of the adsorption structure. For example, in structures II and IV, there are only two new Ti-O bonds between the cluster and the surface and these structures have the least negative adsorption energies. Structures III and IV have more Ti-O bonds and a more negative adsorption energy, while the most stable structure, V, has the largest number of new Ti-O bonds.

In the most stable adsorption structure of Ti$_2$O$_4$, the two Ti atoms are coordinated to bridging oxygen atoms of the surface – one Ti (Ti^A) making bonds to two of these oxygen and the second Ti (Ti^B) making a bond to one bridging oxygen atom, with Ti-O distances of 2.11 and 2.20 Å (Ti^A) and 2.22 Å (Ti^B); figure 4 shows the important geometrical parameters in this supported cluster. The cluster Ti atoms also bond with in-plane oxygen, with Ti-O distances between 2.19 and 2.22 Å. The increased coordination of cluster Ti and O upon adsorption is shown in the Ti-O distances in the cluster. The least affected atom is the terminal oxygen atom that does not bind to the surface – this shows a small increase in its Ti-O distance to 1.68 Å, the other terminal oxygen atom binds to Ti from the surface, and has a Ti-O distance of 1.93 Å, consistent with the Ti-O distance in bulk TiO$_2$.
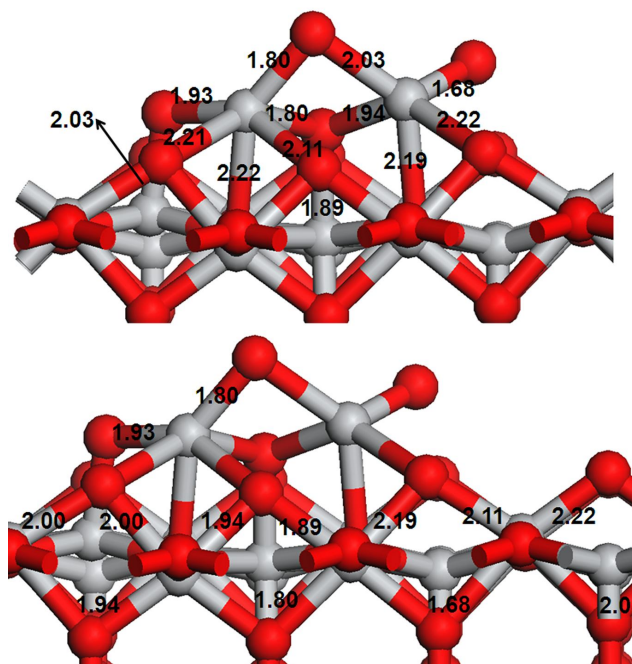

Fig.4 Selected geometry parameters for Ti$_2$O$_4$ supported on rutile TiO$_2$ (110) surface. Each panel shows a selection of Ti-O distances to show more clearly cluster and surface geometry.

For Ti$_3$O$_6$ adsorbed at the (110) surface, we show three stable structures found after relaxation in the top panel of figure 5. The adsorption energies for this cluster are similar in magnitude to those found for Ti$_2$O$_4$ adsorption. In the most stable adsorption structure, structure II, two cluster Ti atoms create bonds with bridging oxygen from the surface. The first Ti bonds to a bridging oxygen atom with Ti-O distance 2.07 Å, while the second Ti bonds with Ti-O distances of 2.04 and 2.12 Å. The same Ti also creates an additional bond to in-plane oxygen atom with a Ti-O distance of 2.23 Å. Moreover two oxygen atoms from the cluster make two bonds with 5-fold coordinated Ti from the surface with Ti-O distances of 1.87 Å and 1.94 Å. The two terminal oxygens of the cluster do not bond to the surface and we observe that their Ti-O distances show a small increase to 1.68 Å, similar to the case of Ti$_2$O$_4$. Figure 6 shows the important geometry parameters and in the cluster and between cluster and surface for Ti$_3$O$_6$.

The 5-fold coordinated Ti from the surface is pulled up by the oxygen from the cluster and the distance in the surface Ti-O is 2.13 Å.
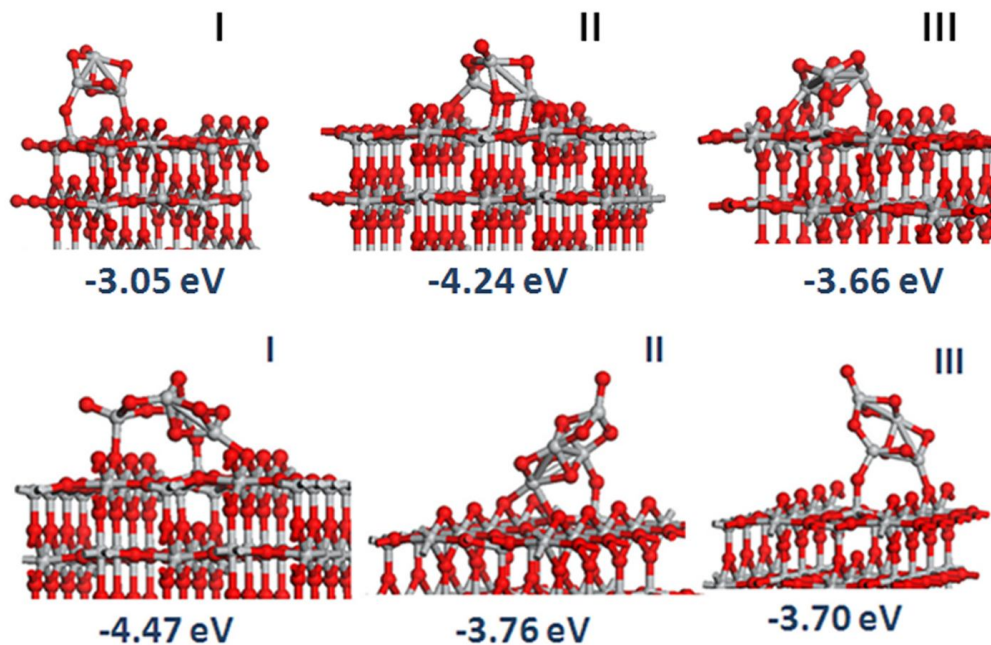

Fig. 5 Relaxed adsorption structures and computed adsorption energies for Ti_3O_6 (top panel) and Ti_4O_8 (bottom panel) deposited on the TiO_2 (110) surface. The roman numerals signify the numbering of the cluster structures. The adsorption energies are given under each structure in eV, computed from eq. (1). The colour scheme is the same as figure 1.

For Ti_4O_8 we show three different adsorption structures in the bottom panel of figure 5. The resulting adsorption energies are similar to those for the Ti_2O_4 and Ti_3O_6 clusters, with structure I being the most stable. The adsorbed cluster is bonded to the surface by three new Ti-O bonds as shown in figure 6: two Ti from the cluster bond to two bridging oxygens from the surface, with Ti-O distances of 1.96 Å and 2.01 Å. One terminal oxygen from the cluster bonds to surface Ti with an increased Ti-O distance of 1.76 Å. The second terminal oxygen does not bond with the surface and again shows a small increase in its Ti-O distance to 1.68 Å. Comparing geometry of free cluster we observe that the adsorbed cluster has only one terminal oxygen with the Ti-O distance 1.66 Å, shown in figure 5. The second terminated Ti atom bonds to Ti from the surface. However other Ti-O distances in the clusters are little affected.
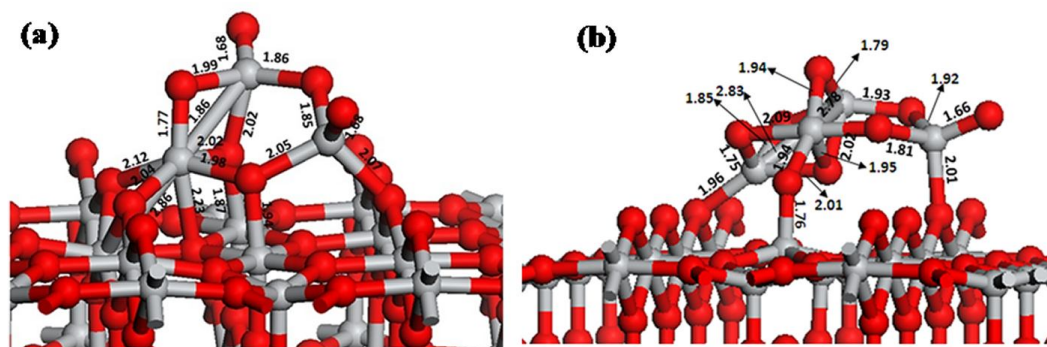

Fig. 6 Geometry data for the most stable Ti_3O_6 (left panel) and Ti_4O_8 (right panel) adsorption structures

3.2 Electronic properties of supported TiO_2 clusters.

The band gap in the present calculations is underestimated for the (110) surface, being 2.1 eV (U = 4.5 eV on Ti), compared to *ca.* 3 eV from experiment. For the clusters we compute with DFT+U band gaps of 2.4 eV, 2.1 eV and 2.8 eV for Ti_2O_4, Ti_3O_6 and Ti_4O_8, respectively. The TiO_2 cluster band gaps do not necessarily follow a monotonic decrease to the bulk value with cluster size, as has been demonstrated in earlier calculations on the bare clusters[1-3,54,55].

For the most stable adsorption configuration of each supported TiO_2 cluster we show the partial electronic density of states (PEDOS) projected onto Ti 3d and O 2p states of both the cluster and the support in figure 7. We have also computed Bader atomic charges on the supported clusters[56].

The first aspect of the electronic structure is that there are no

defect states in the band gap associated with formation of reduced Ti^{3+}. The Bader charges for the (110) surface show a charge on Ti of *ca.* 1.40, while the in the clusters, Ti ions show Bader charges of 1.45 (Ti_2O_4), 1.40 (Ti_3O_6) and 1.40 (Ti_4O_8), so that Ti in the cluster and the surface can be considered oxidised Ti^{4+}.

The second, and key, finding is the makeup of the top of the valence band (VB) and the bottom of the conduction band (CB). The highest occupied states of the cluster lie higher than the VB edge of the surface, as shown in figure 7 for both Ti 3d and, in particular, the O 2p states of the cluster and the surface atoms. This means that the highest occupied VB states of the composite structure are composed of electronic states from the adsorbed TiO_2 cluster. The bottom of the CB is derived from the TiO_2 surface, with the empty electronic states from the cluster lying higher in energy.

Looking briefly at the oxygen 2p PEDOS for individual oxygen atoms, the topmost states of the cluster derived VB edge are derived from the oxygen atoms indicated with blue spheres in the insets of figure 7. These are the oxygen atom(s) of the cluster where the hole produced upon electronic excitation would most likely be trapped. These oxygen atoms are generally undercoordinated atoms in each adsorbed cluster structure, e.g. for Ti_3O_6 and Ti_4O_8, we find that terminal oxygen atoms contribute most to the top of the cluster VB states.

The PEDOS indicates that adsorption of these small clusters on the TiO_2 (110) surface will lead to a reduction in the effective band gap relative to the bare surface. Importantly, the composite structure results in the valence band and conduction band being spatially separated on different parts of the composite system. Thus, electrons and holes formed upon photon absorption will be separated – electrons on the surface and holes on the cluster - and this could be of importance for charge sepration in photocatalysis. Figure 8 shows a schematic of the positions of the valence and conduction band for the composite systems, with the numbers giving the offsets of the surface and cluster VB and CB edges.
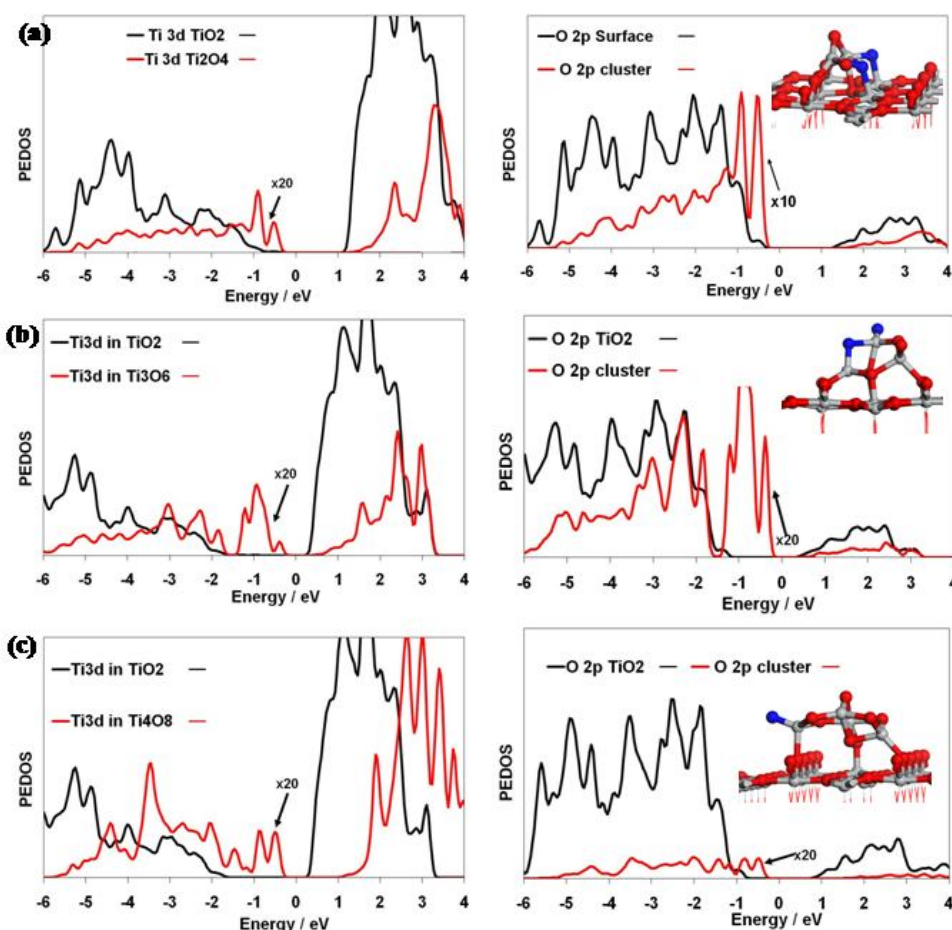

Fig. 7 Electronic density of states projected (PEDOS) on Ti 3d states (left panels) and O 2p states (right panels) for (a) Ti_2O_4 cluster, (b) Ti_3O_6 cluster and (c) Ti_4O_8 cluster supported on the rutile (110) surface.
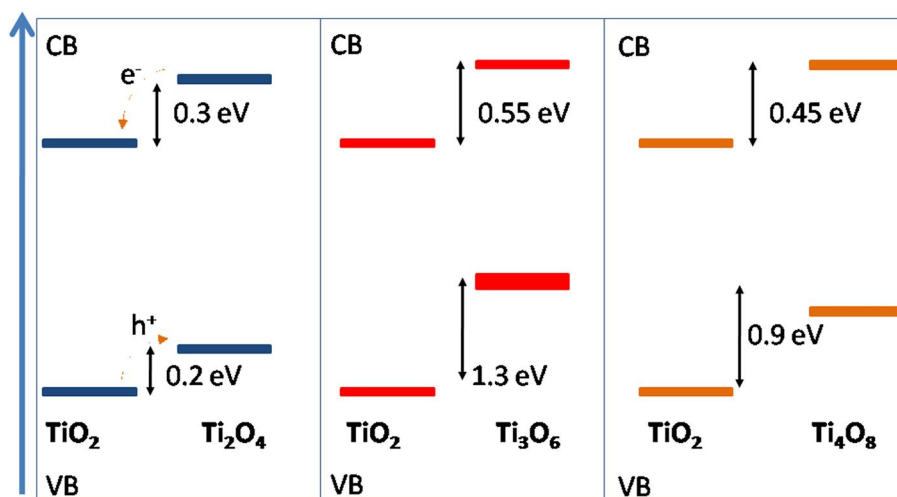
Fig. 8 Schematic diagram showing the VB and CB offsets for the composite systems.

While no experimental information exists for the precise material system in this study, very recent work on FeO$_x$ supported on rutile TiO$_2$ (110)[11] has indicated that the VB and CB are spatially separated, similar to our present findings. Of course, in commercially available TiO$_2$, such as Degussa P25, which is a mix of rutile and anatase TiO$_2$, the separation of valence and conduction bands is well known[57-61]. An interesting recent finding is in ref.[25] in which a composite of doped rutile and doped anatase results in a spatial separation of the composite VB and CB. The composite is demonstrated to show higher photocatalytic acitivity than either of the individual materials. These initial experimental results indicate that these composite systems will be useful for photocatalytic applications.

3.3 Exploring reactivity of supported TiO$_2$ clusters: oxygen vacancy formation

To investigate if the reactivity of the supported clusters is enhanced over the bulk oxide, we have studied the formation of oxygen vacancies on different sites in the three supported clusters. Such knowledge is useful in developing new redox catalysts for reactions such as CO oxidation and NO$_X$ reduction or for the water gas shift reaction. The oxygen vacancy formation energy is considered a good descriptor of how useful a particular material can be for oxidation reactions – the smaller is the vacancy formation energy, the more reactive the oxide will be to oxidation *via* the Mars van Krevelen mechanism[39].

Figure 9 shows the numbering of the different oxygen vacancy sites on each supported cluster. The choice of vacancy sites includes cluster oxygens with different coordination, oxygen shared by the cluster and the surface and the two-fold coordinated bridging oxygen from the surface. In each case, we remove one neutral oxygen atom and allow the structure to relax in response to this change.
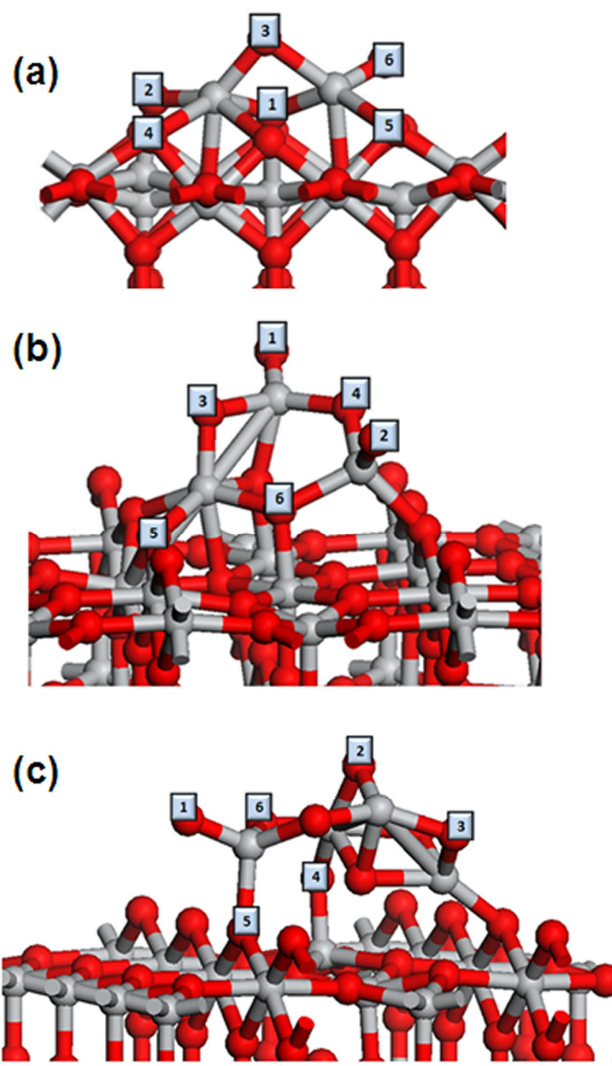

Fig.9 Labelling of the oxygen vacancy sites for adsorbed (a) Ti$_2$O$_4$, (b) Ti$_3$O$_6$, (c) Ti$_4$O$_8$.

Table 1 Oxygen vacancy formation energies, E^{Ovac}, for adsorbed TiO$_2$ clusters from DFT+U. The most stable vacancy site is highlighted in bold font for each supported cluster

O Vacancy Site	1	2	3	4	5	6
Ti$_2$O$_4$ E^{Ovac} / eV	2.87	3.09	3.03	3.08	3.97	**2.54**
Ti$_3$O$_6$ E^{Ovac} / eV	1.53	**0.54**	2.48	0.54	3.93	0.54
Ti$_4$O$_8$ E^{Ovac} / eV	2.13	2.14	---	2.99	1.70	**0.57**

[5] Table 1 presents the oxygen vacancy formation energies for the different oxygen atoms in each supported cluster, while figure 10 shows the most stable oxygen vacancy structures. Other oxygen vacancy structures are shown in the supporting information - as an example to compare DFT and DFT+U [10] results, figures S1 and S2 of the supporting information show the excess spin density computed from DFT and DFT+U in an oxygen vacancy structure for Ti$_2$O$_4$ and Ti$_4$O$_8$ supported on the (110) surface. It is clear that DFT delocalizes the two electrons over many Ti in the surface, as expected, while [15] DFT+U localizes the two electrons on two Ti atoms, which is the correct behaviour[41].

The formation energies show that oxygen vacancy formation is more favourable in the TiO$_2$ clusters than in bulk TiO$_2$ or in the bare (110) surface, for which formation energies are *ca.* [20] 4.2 eV and 3.66 eV, respectively[40-42]. The Ti$_3$O$_6$ and Ti$_4$O$_8$ clusters show especially reduced vacancy formation energies. Thus, the supported cluster will be more reactive than the bulk material oxide which is important for applications in catalysis. We have also healed the most stable oxygen vacacy site in [25] each supported cluster with an oxygen atom and allowed full relaxation in order to investigate if new adsorption structures with potentially higher stability can be obtained, since the defective clusters show some changes in structure and an increase in the number of Ti-O bonds to the support after [30] removal of an oxygen atom. For Ti$_2$O$_4$, we find that structure V (figure 2) is recovered, or a higher energy adsorption structure is found. For the other reduced clusters, Ti$_3$O$_5$ and Ti$_4$O$_7$, we also find either the original adsorption structure or new structures that higher in energy compared to the most [35] stable structure in figure 5.

For the Ti$_2$O$_4$ cluster, the most stable oxygen vacancy structure has a formation energy of 2.54 eV and is shown in figure 10 (a), while the other clusters show formation energies that are quite small, 0.54 – 0.75 eV. This oxygen is a terminal [40] oxygen from the cluster. Interface oxygen atoms show larger formation energies (vacancy sites 1 and 2) and the highest energy cost is for oxygen atoms from the surface (vacancy site 5). One way to understand an origin of these vacancy formation energies is to examine the structures upon [45] relaxation after vacancy formation. In the Ti$_2$O$_4$ cluster, the structure in figure 10(a) is not substantially different to that from the oxidised cluster, so that the structural relaxations after vacancy formation are relatively small. Figure 11 shows the Ti-O distances and the cluster Ti atom neighbouring the [50] oxygen vacancy site shows the largest change in geometry upon vacancy formation.
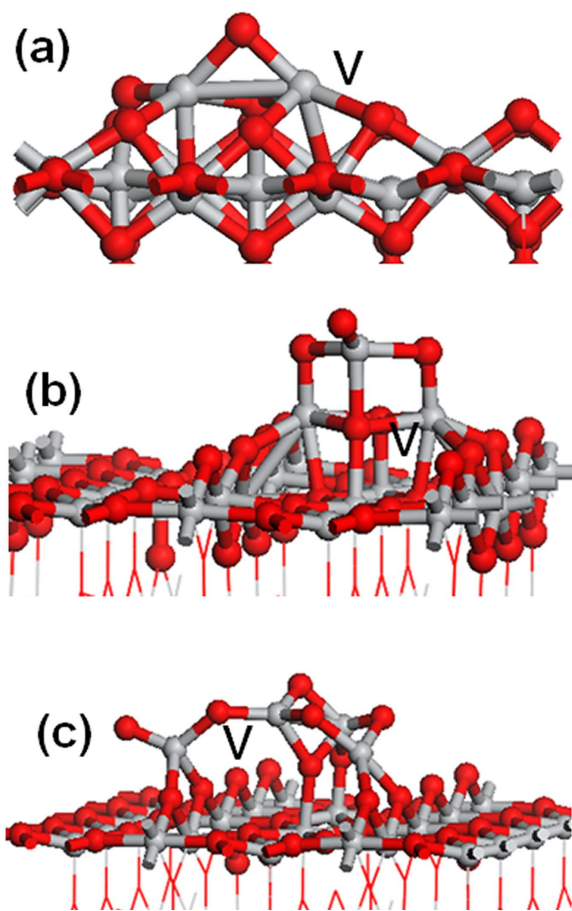

Fig.10 The most stable oxygen vacancy sites for (a) Ti$_2$O$_4$, (b) Ti$_3$O$_6$ and (c) Ti$_4$O$_8$. The "V" on each structure signifies the position of the vacancy [55] site.

In the other clusters, we see notable changes in the structure upon relaxation. For the supported Ti$_3$O$_6$ cluster, sites 2, 4 and 6 in table 1 and figure 9(b) have the same vacancy formation [60] energy. Inspection of the three structures shows that they have the same structure after removal of oxygen, which is mirror symmetric upon removal of O2 in figure 9(b). For oxygen vacancy sites 4 and 6 in figure 9(b), the final structure is obtained by a more complex process in which the oxygen [65] originally at site 2 moves to fill the oxygen vacancy at site 4 or 6, so that ultimately the most stable oxygen vacancy structure is obtained by removing the oxygen at site 2. The relaxed structures from OV4 and OV6 are shown in the supporting information, figure S3. The mirror symmetry in the [70] resulting reduced cluster is apparent from figures 10(b) and 11(b). In addition, there are a number of additional Ti-O bonds formed compared to the oxidised cluster, so that this will stabilize the reduced cluster and hence give a smaller oxygen vacancy formation energy. Comparing the oxidized [75] cluster and reduced cluster, we observe that two Ti atoms from the reduced cluster create more bonds with the surface with the distances Ti-O 2.02 Å (shortest), and 2.22 Å (longest). The reduced cluster has only one terminal O atom with the distance 1.69 Å; the second terminal oxygen was [80] oxygen site 2. There is the same number of 2 coordinated O

atoms with the distances 1.77 Å (shortest), and 1.99 Å (longest) and 3 coordinated O atoms with distances 1.77 Å (shortest), and 2.16 Å (longest).
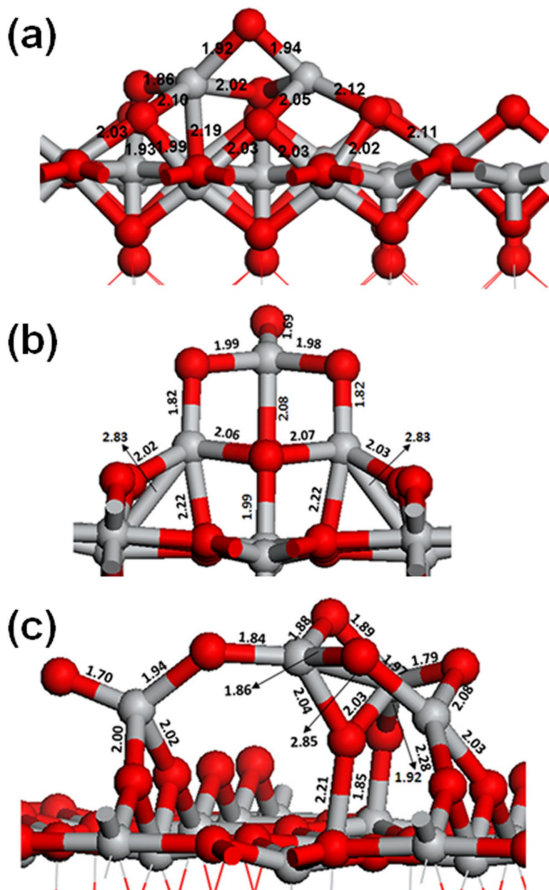

Fig.11 Geometry in the most stable oxygen vacancy structures for (a) Ti_2O_4, (b) Ti_3O_6 and (c) Ti_4O_8.

For Ti_4O_8, the formation of the vacancy also leads to structural relaxations in the cluster and the formation of additional Ti-O bonds between the cluster and the surface, again contributing to enhanced stability of the reduced cluster at the surface and the small vacancy formation energy. We see that oxygen vacancy sites O1 and O2 have very similar vacancy formation energies, but the structures, shown in the supporting information, figure S4, are rather different. The similarity in the oxygen vacancy formation energies is most likely co-incidental.

The most stable reduced Ti_4O_7 cluster creates six Ti-O bonds to the surface while the oxidized cluster only three bonds. Two Ti atoms from the reduced cluster bond to four bridging O atoms from the surface with the Ti-O distances 2.00 Å (shortest), and 2.28 Å (longest) where the Ti from the oxidized cluster bonds to the surface bridging O atom with only two bonds with distances 1.96 Å and 2.01 Å. In both clusters we can find one terminal O atom with Ti-O distance 1.70 Å for the reduced cluster and 1.66 Å for oxidized cluster.

The spin density for the most stable oxygen vacancy structures is shown in figure 12 for each cluster. The spin density is the difference between the up spin and down spin electron density and shows the destination of the the two electrons released by the neutral oxygen vacancy. For each adsorbed cluster the two electrons are localised on two Ti atoms.

On Ti_2O_4 one electron is found in a subsurface Ti site and the second electron is found on a Ti atom from the cluster, indicating that cluster Ti atoms can be reduced. The corresponding Bader charges on these Ti are 1.7 and 1.8 electrons, consistent with formation of Ti^{3+} ions. For the most stable oxygen vacancy in the Ti_3O_6 cluster the two electrons are found in surface Ti sites, with corresponding Bader charges of 1.7 electrons. In Ti_4O_8 one electron is in a subsurface Ti site and the second is on Ti on the cluster and the Bader charges on these Ti are 1.7 electrons. In all cases DFT+U approach localizes the electrons on two Ti^{3+} sites.

The corresponding PEDOS is shown in figure 13 for the three clusters. For each cluster, the PEDOS shows the introduction of electronic states in the band gap after the oxygen vacancy forms. The origin of the gap state depends on the particular cluster structure, but for all structures considered is indicative of formation of reduced Ti^{3+} [40-42], consistent with the spin density plots.

For Ti_2O_4 and Ti_4O_8, one peak in the gap state has its origin in Ti from the cluster, which is the peak nearest the valence band edge. The second peak has its origin in Ti from the supporting oxide, which lies deeper in the gap, at an offset of 0.8 eV from the top of the VB. The two peaks are quite distinct and are separated by ca. 0.7 eV.

The Ti_3O_6 cluster with a vacancy behaves rather differently – its gap state is made up of contributions from two Ti^{3+} ions in the support oxide, as shown in figure 13(c). These are two distinctly different Ti^{3+} species, as can be seen from the spin density plot, and hence they show up as two different peaks in the PEDOS. The highly symmetric structure of the defective Ti_3O_6 cluster prevents a Ti atom of the cluster being reduced, as this would break the symmetry and therefore only surface Ti can be reduced.
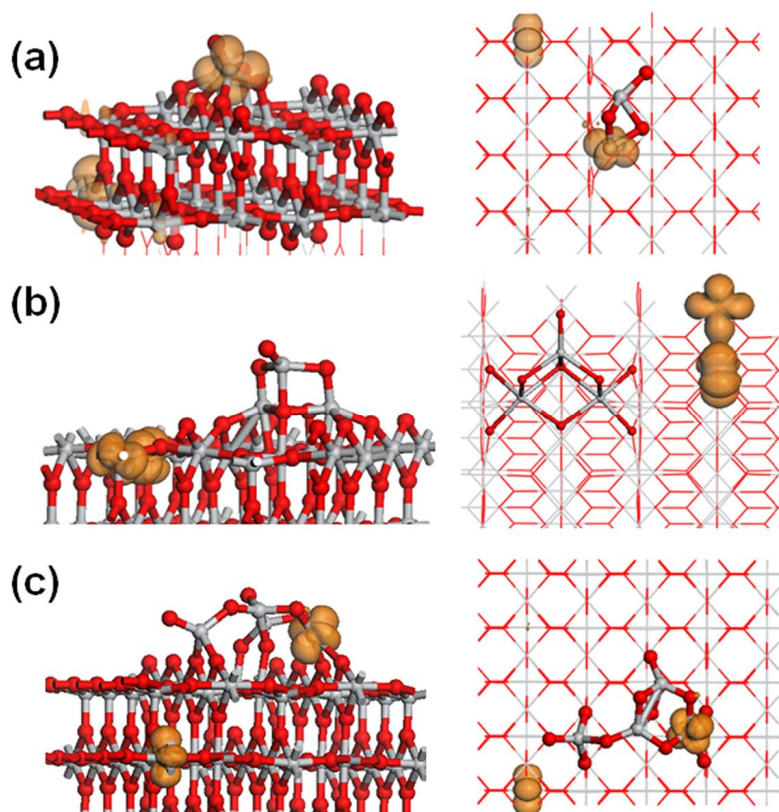
Fig. 12 Spin density for the most stable oxygen vacancy in the supported TiO$_2$ clusters. (a) Ti$_2$O$_4$, (b) Ti$_3$O$_6$, (c) Ti$_4$O$_8$.
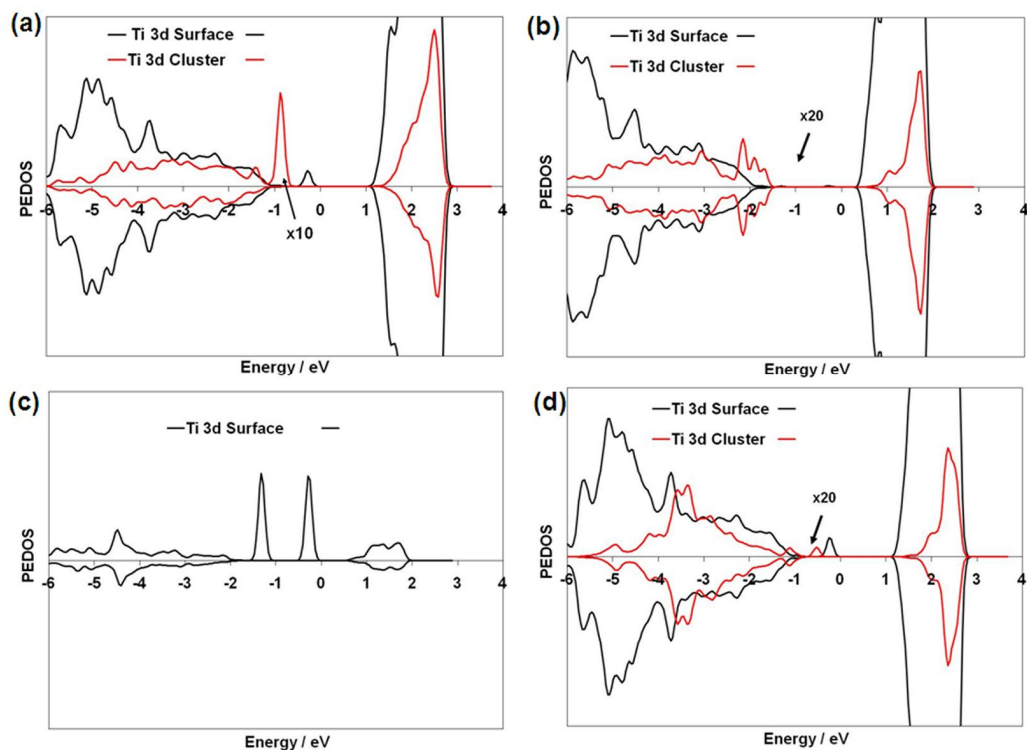

Fig. 13 PEDOS projected onto Ti 3d states for the oxygen vacancy in the supported TiO$_2$ clusters. (a) Ti$_2$O$_4$, (b),(c) Ti$_3$O$_6$, (c) Ti$_4$O$_8$. For Ti$_3$O$_6$, we show in part (c) the PEDOS projected onto the two surface Ti ions carrying the spin density from figure 12, as their PEDOS is swamped by the contributions from the remaining Ti of the TiO$_2$ support.

4. Conclusions

Metal oxide clusters of-sub nm dimensions dispersed on a metal oxide support are a key class of catalytic materials and also show promise for photocatalytic applications. The results of a density functional theory study of small sub-nm scale TiO_2 clusters, Ti_2O_4, Ti_3O_6 and Ti_4O_8 deposited at the rutile (110) surface show the following:

(i) all clusters adsorb strongly in a number of adsorption configurations, with adsorption energies ranging from -3 eV to -4.5 eV.

(ii) the more stable adsorption structures show a larger number of new Ti-O bonds formed between the cluster and the surface.

(iii) the electronic structure shows that the valence band edge is derived from cluster electronic states and the conduction band edge is made up of surface electronic states

(iv) a reduction in the effective band gap and spatial separation of electrons and holes after photon absorption is predicted

(v) to examine reactivity, oxygen vacancy formation was studied and the most stable oxygen vacancy sites are on the cluster, showing reduced formation energies compared to the bulk oxide and making them potentially useful in redox catalysis.

These results show that supported oxide nanoclusters have great potential as materials in photocatalysis and redox catalysis.

Acknowledgements

Notes and references

b Tyndall National Institute, University College Cork, Lee Maltings, Cork, Ireland
E-mail: michael.nolan@tyndall.ie

1. S. Hamad, C. R. A. Catlow, S. M. Woodley, S. Lago and J. A. Mejias, *J. Phys. Chem. B* 2005, **109**, 15741
2. M. Calatayud and C. Minot, *J. Phys. Chem. C*, 2009, **113**, 12186
3. M. Calatayud, L. Maldonado and C. Minot, *J. Phys. Chem. C*, 2008, **112**, 16087
4. Z-W. Qu and G-J Koes, *J. Phys. Chem. C*, 2007, **111**, 16808
5. O. Bondarchuk, X. Huang, J. Kim, B. D. Kay, L. S. Wang, J. M. White and Z. Dohnalek, *Angew. Chem., Int. Ed.*, 2006, **45**, 4786
6. J. A. Rodriguez and J. Hrbek, *Surf. Sci.*, 2009, **604**, 241
7. J. A. Rodriguez and D. Stacchiola, *Phys. Chem. Chem. Phys.*, 2010, **12**, 9557
8. T. Onfroy, G. Clet and M. Houalla, *J. Phys. Chem. B*, 2005, **109**, 14588
9. L Barrio, M. Estrella, G. Zhou, W. Wen, J. C. Hanson, A. B. Hungria, A. Hornes, M. Fernandez-Garcia, A. Martinez-Arias and J. A. Rodriguez *J. Phys. Chem C*, 2010, **114**, 3580
10. H. Irie, S. Miura, K. Kamiya and K. Hashimoto, *Chem. Phys. Lett.*, 2008, **456**, 202
11. J. A. Libera, J. W. Elam, N. F. Sather, T. Rajh and N. M. Dimitrijevic, *Chem. Mat.*, 2010, **22**, 409
12. S. D. Tilley, M. Cornuz, K. Sivula and M. Graetzel, *Angew. Chem. Intl. Ed.*, 2010, **49**, 6405
13. M. Moreno, L. Bergamini, G. T. Baronetti, M. A. Laborde and F. J. Marino, *Int. J. Hydrogen Energ.*, 2010, **35**, 5918
14. M. Baron, H. Abbott, O. Bondarchuk, D. Stacchiola, A. Uhl, S. Shaikhutidinov, H-J. Freund, C. Pop, M. V. Ganduglia-Pirovano,and J. Sauer, *Angew. Chem. Int. Ed.*, 2009, **48**, 8006
15. J. E. Molinari and I. E. Wachs, *J. Am. Chem, Soc.*, 2010, **132**, 12559
16. L. J. Burcham, G. Deo, X. Gao and I. E. Wachs, *Top. Catal.*, 2000, **11/12**, 85
17. X. Gao, S. R. Bare, B. M. Weckhuysen and I. E. Wachs, *J. Phys. Chem. B*, 1998, **102**, 10842
18. J. Kim, O. Bondarchuk, B. D. Kay, J. M. White and Z. Dohnalek, *Catal. Today*, 2007, **120**, 186
19. J. B. Park, J. Graciani, J. Evans, D. Stacchiola, S. Ma, P. Liu, A. Nambu, J. F. Sanz, J. Hrbek and J. A. Rodriguez, *P. Natl. Acad. Sci.*, 2009, **106**, 4975
20. J. B. Park, J. Graciani, J. Evans, D. Stacchiola, S. D. Senanayake, L. Barrio, P. Liu, J. F. Sanz, J. Hrbek and J. A. Rodriguez, *J. Am. Chem. Soc.*, 2010, **132**, 356
21. T. Onfroy, O. Manoilova, S. B. Bukallah, D. M. Hercules, G. Clet and M. Houalla, *Appl. Cat. A*, 2007, **316**, 184
22. T. Onfroy, O. Manoilova, S. B. Bukallah, D. M. Hercules, G. Clet and M. Houalla, *Appl. Cat. A*, 2006, **298**, 80
23. N. Soultanidis, W. Zhou, A. C. Psarras, A. J. Gonzalez, E. F. Illiopoulou, C. J. Kiely, I. E. Wachs and M. S. Wong, *J. Am. Chem. Soc.*, 2010, **132**, 13462
24. L. Peng, T. Xie, Y. Lu, H. Fan and D. Wang *Phys. Chem. Chem. Phys.*, 2010, **12**, 8033
25. Y. Cao, T. He, Y. Chen and Y. Cao, *J. Phys. Chem. C*, 2010, **114**, 3627
26. V. Etacheri, M. K. Seery, S. J. Hinder and S. C. Pillai, *Chem. Mat.*, 2010, **22**, 3843
27. J. Graciani, J. Plata, J. F. Sanz, P. Liu and J. A. Rodriguez, *J. Chem. Phys.*, 2010, **132**, 104703
28. J. Zhu, H. Jin, W. Chen, Y. Li, Y. Zhang, L. Ning, X. Huang, K. Ding and W. Chen., *J. Phys. Chem. C*, 2009, **113**, 17509
29. H. Y. Kim, H. M. Lee, R. G. S. Pala and H. Metiu, *J. Phys. Chem. C*, 2009, **113**, 16083
30. H. Y. Kim, H. M. Lee, R. G. S. Pala, V. Shapovalov and H. Metiu, *J. Phys. Chem. C*, 2009, **113**, 12398
31. L. Cheng, D. Mei and Q. Ge, *J. Phys. Chem. C*, 2009, **113**, 18296
32. A. Vittadini, M. Casarin and A. Selloni, *J. Phys. Chem. B*, 2005, **109**, 1652
33. V. Shapovalov and H. Metiu, *J. Phys. Chem. C*, 2007, **111**, 14179
34. M. Calatayud and C. Minot, *Top. In Cat.*, 2006, **40**, 17
35. N. A. Deskins, S. Kerisit, K. M. Rosso and M. Dupuis, *J. Phys. Chem., C*, 2007, **111**, 9290
36. V. Shapovalov and H. Metiu, *J. Cat.*, 2007, **245**, 205
37. M. Nolan, *J. Phys. Chem. C*, 2009, **113**, 2425
38. B. Li and H. Metiu, *J. Phys. Chem. C*, 2010, **114**, 12234
39. P. Mars and D. W. van Krevelen, *Special Suppl. Chem. Eng. Sci.* 1954, **3**, 41.
40. B. J. Morgan and G. W. Watson, *Surf. Sci.*, 2007, **601**, 5034
41. M. V. Ganduglia-Pirovano, A. Hofmann and J. Sauer, *Surf. Sci. Rep.*, 2007, **62**, 219
42. C. Di Valentin, G. Pacchioni and A. Selloni, *Phys. Rev. Lett.*, 2006, **97**, 166803
43. A. Migani, G. N. Vayssilov, S. T. Bromley, F. Illas and K. M. Neyman, *Chem. Commun.* 2010, **46**, 5963
44. G. Kresse and J. Hafner, *Phys. Rev. B* 1994, **49**, 1425
45. P. E. Blöchl, *Phys. Rev. B* 1994, **50**, 17953
46. J. P. Perdew, in: Ziesche, P.; Eschrig H. (Eds.), *Electronic Structure of Solids '91*, Akademie Verlag, Berlin, 1991
47. M. Nolan, S. D. Elliott, R. A. Bennett, J. S. Mulley, M. Basham and P. A. Mulheran, *Phys. Rev. B*, 2008, **77**, 235424

48. V. I. Anisimov, J. Zaanen and O. K. Andersen, *Phys. Rev B* 1991**, 44** 943

49. S. L. Dudarev, G. A. Botton, S. Y. Savrasov, C. J. Humphreys and A. P. Sutton, *Phys. Rev. B,* 1998**, 57***, 1505

50. M. Nolan, S. Grigoleit, D. C. Sayle, S. C. Parker and G. W. Watson, *Surf. Sci.,* 2005, **576**, 217

51. D. O. Scanlon, A. Walsh, B. J. Morgan, M. Nolan, J. E. Fearon and G. W. Watson, *J. Phys. Chem. C*, 2007, **111**, 7971

52. B. J. Morgan and G. W. Watson, *J. Phys. Chem. C,* 2009, **113**, 7322

53. C. J. Calzado, N. C. Hernández and J. F. Sanz, *Phys. Rev. B* 2008**, 77**, 045118

54. M. Calatayud and C. Minot, *J. Phys. Chem.* C 2009, **113,** 12186

55. S. A. Shevlin and S. M. Woodley, *J. Phys. Chem. C* 2010, **114,** 17333

56. G. Henkelman, A. Arnaldsson and H. Jónsson, *Comput. Mater. Sci.* 2006**, 36**, 254

57. L. Zhao, M. Han and J. Lian, 2008, **516**, 3394

58. D. C. Hurumm, A. G. Agrios, K. A. Gray, T. Rajh and M. C. Thurauner, *J. Phys. Chem. B*, 2003, **107**, 4545

59. T. Ohno, K. Sarukawa and M. Matsumura, *New. J. Chem.*, 2002, **26**, 1167

60. Y. Zhang, J. Cheng and X. Li, *Cat. Lett.,* 2010, **139**, 129

61. W. Lee, Y. R. Doo, K. Dwight and A. Wold, *Mat. Res. Bull.,* 1993, **28**, 1127